Experimental Observation of Critical Scaling in Magnetic Dynamic Phase Transitions

M. Quintana● and A. Berger●*

CIC nanoGUNE BRTA, E-20018 Donostia–San Sebastián, Spain

We explore the critical behavior of dynamic phase transitions in ultrathin uniaxial Co films. Our data demonstrate the occurrence of critical fluctuations, which define the critical regime, and in which we conduct a scaling analysis of the dynamic order parameter Q, utilizing a dynamic analog to the Arrott-Noakes equation of state. Our results show dynamic critical exponents that agree with the 2D Ising model as theoretically predicted. However, equilibrium critical exponents of our sample agree with the 3D Ising model. We argue that these differences between dynamic and thermodynamic behavior are due to fundamentally different length scales at which dimensional crossovers occur.

Nonequilibrium phase transitions are known to happen in a wide array of physical systems [1], such as superconducting materials [2], charge density waves [3], or mechanical crack propagations [4,5], among others [6–8]. One particularly intriguing example of such phenomena is the dynamic phase transition (DPT) of ferromagnetically ordered materials at temperatures below their Curie temperature T_C [9]. Most relevantly, the DPT exhibits strong similarities with the conventional thermodynamic phase transition (TPT) in equilibrium, including the expected scaling behavior [10]. This in turn has attracted widespread attention in the scientific community [11–15] as it enables the use of powerful methods toward the description of nonequilibrium phenomena originally envisioned for equilibrium systems only [16]. Unfortunately, a complete lack of experimental verifications has impeded further progress. Accordingly, providing experimental evidence for DPT scaling behavior is the primary purpose of this work.

At the DPT, the dynamic magnetization trajectory $M(t)$ undergoes qualitative changes upon varying the period P of an oscillating magnetic field $H(t)$. These changes are characterized by the dynamic order parameter, defined as

$$Q = \frac{1}{P} \int_t^{t+P} M(t')dt', \qquad (1)$$

whose behavior implies a second order phase transition (SOPT) at a unique critical period P_c. This qualitative change in dynamic behavior is displayed in Figs. 1(a) and 1(b) by two representative $M(t)$ curves, which were computed using a mean-field approximation model in the presence of a sinusoidal $H(t)$ of fixed amplitude H_0 and periods $P > P_c$ and $P < P_c$, respectively [17]. Both M trajectories exhibit very different behavior because for faster dynamics, shown in Fig. 1(b), $M(t)$ cannot follow the field oscillations. This leads to fundamentally different values of Q, represented in Figs. 1(a) and 1(b) as

green-dashed lines. The computed Q vs P dependence is shown in Fig. 1(c), identifying the SOPT at P_c, which separates the dynamic paramagnetic (PM) phase, from the dynamic ferromagnetic (FM) phase [17]. Theoretically, Q is known to exhibit scaling in the vicinity of the SOPT, specifically

$$Q \propto (P_c - P)^{\beta_d}, \quad \text{for } P < P_c, \qquad (2)$$

where β_d is a dynamic critical exponent [18,19].

A constant bias field H_b, superimposed to the field oscillations, represents the conjugate field of Q [20–25],
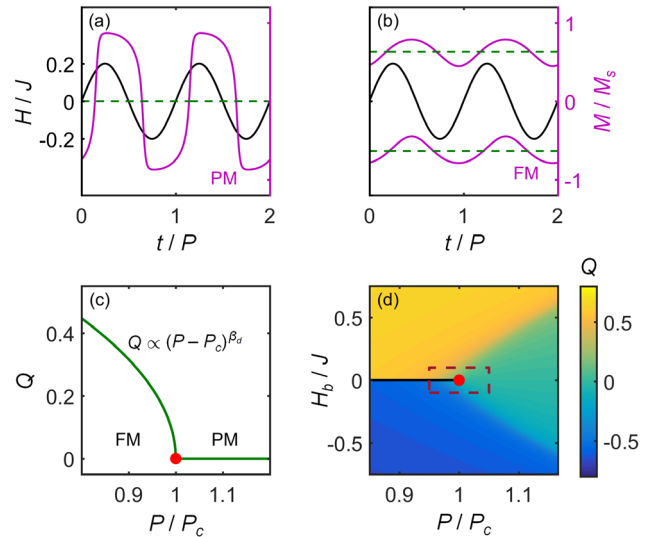

FIG. 1. Mean-field approximation calculation results of $M(t)$ (magenta) in the presence of an oscillatory $H(t)$ (black) for $P > P_c$ (a) and $P < P_c$ (b) with the green-dashed lines representing Q. (c) Q vs P behavior, showing SOPT type behavior at $P = P_c$. (d) Color-coded map representing $Q(P, H_b)$ in the phase-space vicinity of P_c. The dark-red box represents the region in which scaling according to the Eqs. (2) and (3) is expected theoretically.

analogous to a static field H being the conjugate field of M in equilibrium [26]. The stable states of Q in the (P, H_b) phase space are shown as a color-coded map in Fig. 1(d). Here, for $P < P_c$, Q shows two stable states, characterized by the yellow and blue regions of the map. In this region, Q undergoes an abrupt reversal, characterized by a first order phase line at $H_b = 0$, and illustrated by a black line that ends at the SOPT, displayed as a red dot. In the PM phase, for $P > P_c$, Q changes continuously as a function of H_b [27,28]. Theoretical studies have identified a field scaling relation [24],

$$Q \propto H_b^{1/\delta_d}, \quad \text{for } P = P_c, \qquad (3)$$

where $\delta_d = 1 + \gamma_d/\beta_d$ and γ_d are additional dynamic critical exponents. Equations (2) and (3) show fundamentally identical scaling behavior for the DPT and TPT, where $M \propto (T_C - T)^\beta$ for $T < T_C$ and $M \propto H^{1/\delta}$ for $T = T_C$, with β, $\delta = 1 + \gamma/\beta$ being the exponents of the TPT. Furthermore, all theoretical studies point toward fundamentally identical critical exponents, with $\beta_d = \beta$, $\gamma_d = \gamma$, and $\delta_d = \delta$ [15,16,29–31]. However, no experiment has confirmed this crucial aspect to date.

This absence of experimental data is primarily associated with the existence of metamagnetic anomalies near the DPT that do not exist in thermal equilibrium. Especially the PM phase behavior of Q is massively deformed due to anomalous metamagnetic fluctuations that extend to the immediate vicinity of the critical point and constrain the scaling regime to a very limited parameter space [10,27,28]. Correspondingly, a key part of our preliminary experimental work has been the identification of a suitable sample type in which metamagnetic anomalies are sufficiently weak [32].

For this study, we fabricated a series of thin Co $(10\underline{1}0)$ films in the thickness range of 0.7–20 nm [40] and measured their DPT characteristics. All our samples exhibit a DPT, but the present work focuses on a sample with 0.8 nm thickness only. This film is sufficiently thin so that it can be expected to exhibit 2D Ising-like behavior, while also exhibiting $T_C > 300$ K, which is crucial for our high-sensitivity magneto-optical measurement technique that requires in air, room-temperature measurements. The key aspect of this film is, however, that in contrast to thicker films, it does not exhibit relevant metamagnetic anomalies, as we will demonstrate in conjunction with Fig. 2 [32]. The crystal structures of our Co (10_10) films exhibit an in-plane uniaxial magnetic easy axis along the (0001) direction, mimicking the Ising model's bimodal magnetization state behavior, also because dipolar interactions are extremely weak in this geometry [22,25,41,42].

We measure the real-time dynamic behavior of our films by means of an ultrasensitive transverse magneto-optical Kerr effect setup [43–47], whose details were reported in [42]. In our experiments, we determine both
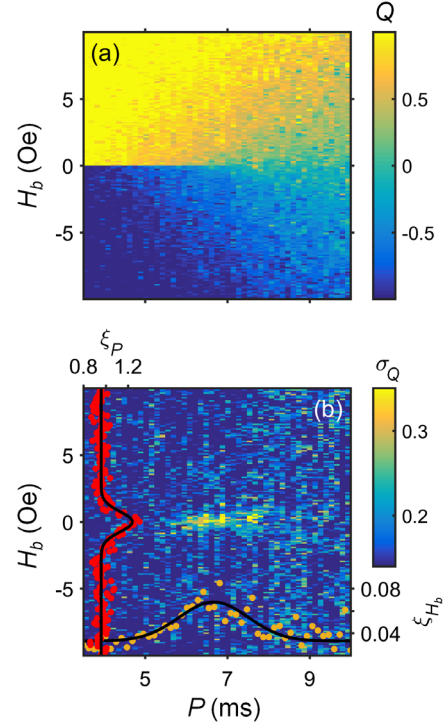

FIG. 2. (a) Color-coded map of experimental $Q(P, H_b)$ data for $H_0 = 47.6$ Oe. (b) Color-coded map of experimental $\sigma_Q(P, H_b)$ data in the same (P, H_b) region showing large fluctuations close to P_c. The line-plot insets represent the statistical evaluation of ξ_p (red) and ξ_{H_b} (orange) with the black lines representing Gaussian fits to the experimental data.

the average values of Q and the dynamic fluctuations $\sigma_Q = \sqrt{\langle Q^2 \rangle - \langle Q^2 \rangle}$ throughout the (P, H_b) phase space in the vicinity of P_c by measuring signal traces under identical field sequence conditions [22,41,42]. Given the monotonously decreasing P_c vs H_0 dependence, we can adjust the field amplitude so that P_c is in the millisecond range. This ensures that we can measure both Q and σ_Q with sufficiently high signal-to-noise ratios near the DPT point. Figure 2(a) shows as a color-coded map the Q phase-space behavior in the vicinity of the critical point for $H_0 = 47.6$ Oe. As explained in connection with Fig. 1(d), two states are observed with opposite $\pm Q$ values in the FM phase, for positive and negative H_b, respectively, separated by a phase line at $H_b = 0$ Oe. In the PM phase, Q changes as expected in a continuous fashion [8], demonstrating that we can experimentally observe Q near the DPT for our ultrathin film.

To investigate the scaling behavior of Q, we need to first identify the critical regime near P_c. Correspondingly, we have analyzed experimental σ_Q values in the same phase-space region, shown in Fig. 2(b). Here, we observe enhanced σ_Q values close to the SOPT, verifying the existence of critical fluctuations in an approximately ellipse-shaped yellow region in the center of the figure. Our statistical analysis of the σ_Q values along the P and H_b

axes, calculated as $\xi_{H_b} = \int \sigma_Q dP$ and $\xi_P = \int \sigma_Q dH_b$, respectively, enables us to quantify the region that exhibits DPT associated fluctuations as displayed in Fig. 2(b). The data in Fig. 2(b) reveal that the ξ_{H_b} and ξ_P peaks exhibit standard deviations $\Delta H = 1.07$ Oe and $\Delta P = 1.2$ ms, respectively. For our subsequent quantitative analysis, we employ a $\pm 3\Delta H$ and $\pm 3\Delta P$ phase-space criterion surrounding the critical point for our scaling behavior analysis of Q. Crucially, our data also verify that in this particular sample with only 0.8 nm thickness, no relevant metamagnetic fluctuations occur in the PM phase, so that these anomalies cannot impact our scaling analysis. In thicker films, however, we find significant metamagnetic fluctuations to be always present [32].

Figure 3 shows our analysis of the Q scaling behavior. Figures 3(a)–3(c) show as color-coded maps the relevant phase-space behavior of Q for three independent datasets, measured for three different H_0 values. All cases exhibit well-distinguished FM and PM phases. We also observe the expected decrease of P_c with H_0 [10]. In order to verify the scaling behavior of our data according to Eqs. (2) and (3), we now assume that they fulfill the dynamic analog to the Arrott-Noakes equation of state [48],

$$\left(\frac{H_b}{Q}\right)^{1/\gamma_d} = \frac{P - P_c}{P_1} + \left(\frac{Q}{Q_1}\right)^{1/\beta_d}, \quad (4)$$

with P_1 and Q_1 being material specific constants. If scaling behavior similar to the TPT case exists for the DPT, Eq. (4) should precisely describe $Q(P, H_b)$ in the vicinity of P_c. To the best of our knowledge, such an Arrott-Noakes equation-of-state approach has not been explored so far in conjunction with the DPT. For our analysis, we also considered the existence of narrow P_c distributions representing lateral film variations and characterized by an average critical point $\widetilde{P_c}$ and associated standard deviation ΔP_c [32,48–51]. In Figs. 3(d)–3(f), we show the least-squares fittings of Eq. (4) to our data. Here, we observe that not only the core characteristics of $Q(P, H_b)$ are precisely reproduced in all cases, but that the fit function is in excellent quantitative agreement with the experimental data. To confirm this, we show in Figs. 3(g)–3(i) the residual differences between experimental data and fits to Eq. (4). Here, we observe no systematic deviations, but only white noise in the entire analyzed phase space, validating our analysis approach.

Our data analysis now enables us to generate scaling plots of properly renormalized Q, given by $|Q/Q_1|/|p|^{\beta_d}$, versus the renormalized bias field $|H_b|/|p|^{\beta_d+\gamma_d}$, with $p = (P - \widetilde{P_c})/P_1$ [32]. Here, all the points in the phase space should collapse onto two different curves corresponding to the PM and FM phases [48]. The results of this analysis are represented in Figs. 3(j)–3(l), and we find that
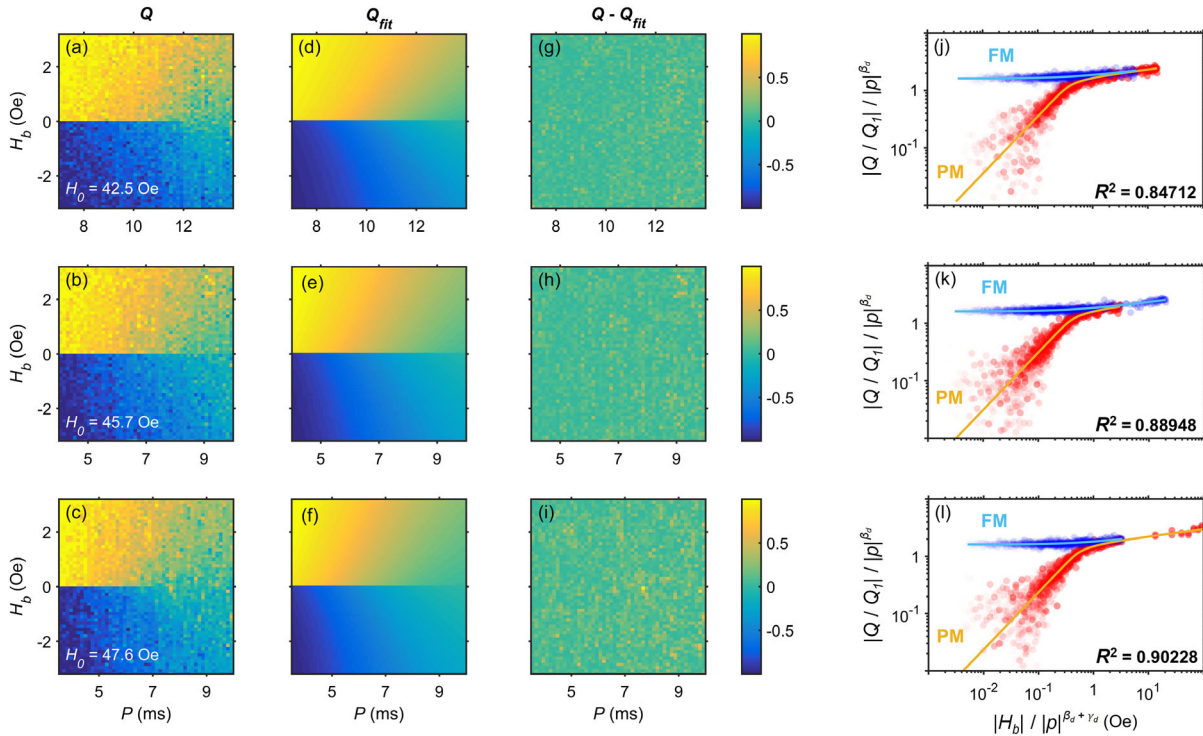

FIG. 3. (a)–(c) Color-coded maps of experimental $Q(P, H_b)$ data for three different H_0 in the critical region. (d)–(f) Color-coded maps of $Q_{\text{fit}}(P, H_b)$ obtained from fits of Eq. (4) to the data in (a)–(c). (g)–(i) Color-coded maps of $Q - Q_{\text{fit}}(P, H_b)$. (j)–(l) Arrott plots of the renormalized order parameter $|Q/Q_1|/|p|^{\beta_d}$ as a function of the renormalized field $|H_b|/|p|^{\beta_d+\gamma_d}$, showing the collapse onto two different curves corresponding to the FM (blue) and PM (red) phases. The cyan and orange lines represent the ideal behavior.

TABLE I. Critical exponents and associated fit parameters extracted from the experimental DPT and TPT data analysis.

H_0 (Oe)	β_d	γ_d	P_c (ms)	ΔP_c (ms)	R^2
42.5 ± 0.1	0.13 ± 0.03	1.0 ± 0.1	10.2 ± 0.5	2.9 ± 0.1	0.8471
45.7 ± 0.1	0.14 ± 0.03	1.1 ± 0.2	6.5 ± 0.4	3.0 ± 0.3	0.8894
47.6 ± 0.1	0.14 ± 0.04	1.0 ± 0.1	5.6 ± 0.4	2.9 ± 0.2	0.9022
	β	γ	T_C (K)	ΔT_C (K)	
TPT experiment	0.325 ± 0.009	1.39 ± 0.05	369.9 ± 0.2	13.0 ± 0.2	0.9980
2D Ising	0.125	1.75			
3D Ising	0.3264	1.237			

all data collapse onto two branches, corresponding to FM (cyan) and PM (orange) dynamic phases. Hereby, our data extend over four decades in the renormalized field and about two decades in the renormalized order parameter. Furthermore, we report $R^2 > 0.84$ values for all data fits.

Our quantitative analysis results in an average critical exponent $\beta_d = 0.137 \pm 0.019$, which is in very good agreement with the critical exponent of the 2D Ising Model (see Table I). We also observe that the results for γ_d show rather significant deviations from the 2D Ising model, a fact that we believe to be associated with the extremely sharp onset of Q at very low H_b values. Here, our experimental field resolution is limited by the noise level with which we can keep H_0 and H_b constant and, thus, the H_b axis is difficult to access experimentally with yet higher precision.

In order to compare the critical exponents of the DPT and TPT, we conducted the corresponding thermodynamic study on the same sample by measuring M as a function of T and H, as shown in Fig. 4. We clearly observe the SOPT at $T_C = 369.9$ K in our experimental SQUID data shown in the inset of Fig. 4, which allows us to accurately quantify the critical regime of the TPT. We fit those data to the Arrot-Noakes equation of state [48] and obtain
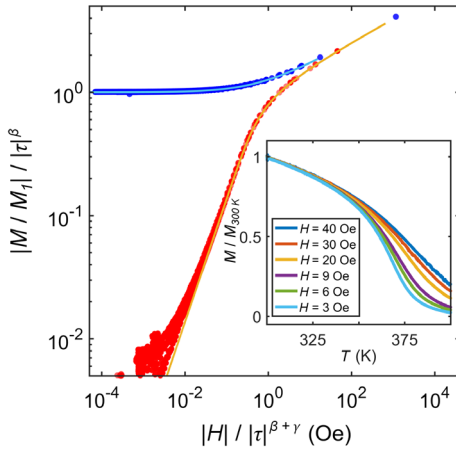

FIG. 4. Arrott plot of renormalized magnetization $|M/M_1|/|\tau|^\beta$ data as a function of the renormalized field $|H|/|\tau|^{\beta+\gamma}$. The inset figure represents the measured $M(T, H)$ data.

excellent scaling ($R^2 = 0.9980$) as seen in the main plot of Fig. 4, which displays the renormalized magnetization $|M/M_1|/|\tau|^\beta$ plotted versus the renormalized field $|H|/|\tau|^{\beta+\gamma}$, with $\tau = (T - \widetilde{T_C})/T_1$. This plot exhibits two separate curves representing the PM and FM phases in analogy to Figs. 3(j)–3(l). The results from this procedure lead to critical exponents of $\beta = 0.325 \pm 0.009$ and $\gamma = 1.39 \pm 0.05$, which actually agree with those of the 3D Ising model, as seen in Table I.

The above results suggest that DPT and TPT exhibit fundamentally different dimensionalities, which is a confusing result, given that the measurements were conducted on the same sample. In order to explain this seeming contradiction, we must have a closer look at our experimental system. It is known from prior experimental studies of the TPT that critical exponents transition from the 2D to the 3D case in the 4–11 monolayer thickness range [52–55] upon using a constant relative temperature range. This is because such magnetic films show a dimensional crossover of criticality from a 3D behavior away from the immediate vicinity of T_C toward 2D properties extremely close to T_C, when the true 2D nature of a film becomes apparent in its fluctuations. Thus, our thermodynamic measurements show the frequently appearing 3D behavior of thin magnetic film in this thickness range.

Our observation of 2D dynamic critical exponents must then be related to a different crossover point, at which the 2D to 3D transition occurs. The nonequilibrium reversal of our films is dominated by nucleation processes, for which the domain-wall (DW) width is estimated to be about 100 nm [56], which is 2 orders of magnitude larger than the thickness. Therefore, dynamic nucleation formation and subsequent DW expansion happen purely in a 2D manner in our sample. Thus, our experimental observations suggest two fundamentally different length scales for the TPT and DPT at which dimensional crossovers occur for finite-thickness films. While perpendicularly magnetized systems, such as Co/Pt multilayers, can exhibit significantly lower DW widths, and thus would in principle allow for more comparable crossover length scales, such systems are generally not suitable for DPT observations due to a loss of

bistable dynamical behavior caused by strong dipolar interactions [21]. To the best of our knowledge, the subject of dimensional crossover has not been studied theoretically with respect to the DPT. Potentially, it might also be related to the anomalous surface behavior of the DPT [57].

In this Letter, we experimentally explored the scaling behavior and critical exponents of the DPT in ultrathin Co films. Our measurements demonstrate the occurrence of critical fluctuations and allowed us to experimentally identify the critical regime. For the quantitative scaling analysis, we propose and utilize the dynamic equivalent of the Arrott-Noakes equation of state. Our data analysis shows excellent quantitative agreement with this approach and reveals that the critical exponents of the DPT agree with those of the 2D Ising model, which was the key purpose of our study. We also observe that the thermodynamic critical exponents of our sample agree with the 3D Ising case instead, causing a discrepancy between TPT and DPT critical exponents, a fact that we associate with fundamentally different length scales at which dimensional crossover occurs for finite thickness magnetic films.

---

[*]Corresponding author: a.berger@nanogune.eu

[1] M. Henkel, H. Hinrichsen, and S. Lübeck, *Non-Equilibrium Phase Transitions: Volume 1: Absorbing Phase Transitions (Theoretical and Mathematical Physics)* (Springer, USA, 2008), ISBN 978-1402087646, 10.1007/978-1-4020-8765-3.

[2] P. H. Kes, N. Kokubo, and R. Besseling, Physica (Amsterdam) **408-410C**, 478 (2004).

[3] N. Ogawa, Y. Murakami, and K. Miyano, Phys. Rev. B **65**, 155107 (2002).

[4] D. Bonamy, S. Santucci, and L. Ponson, Phys. Rev. Lett. **101**, 045501 (2008).

[5] A. Shekhawat, S. Zapperi, and J. P. Sethna, Phys. Rev. Lett. **110**, 185505 (2013).

[6] M. Takayasu, H. Takayasu, and K. Fukuda, Physica (Amsterdam) **277A**, 248 (2000).

[7] A. Zong *et al.*, Phys. Rev. Lett. **123**, 097601 (2019).

[8] F. Carollo and I. Lesanovsky, Phys. Rev. Lett. **128**, 040603 (2022).

[9] T. Tomé and M. J. de Oliveira, Phys. Rev. A **41**, 4251 (1990).

[10] P. Riego, P. Vavassori, and A. Berger, Physica (Amsterdam) **549B**, 13 (2018).

[11] X. Shi and P. Liu, Physica (Amsterdam) **536A**, 120998 (2019).

[12] M. Acharyya, Phys. Rev. E **69**, 027105 (2004).

[13] E. Vatansever, Physica (Amsterdam) **511A**, 232 (2018).

[14] Y. Yüksel, Physica (Amsterdam) **580A**, 126172 (2021).

[15] A. Vasilopoulos, Z. D. Vatansever, E. Vatansever, and N. G. Fytas, Phys. Rev. E **104**, 024108 (2021).

[16] C. Campajola, F. Lillo, P. Mazzarisi, and D. Tantari, J. Stat. Mech. (2012) 033412.

[17] In our mean-field calculations, $H(t)$ is normalized to the exchange energy J and P is normalized to a relaxation time constant τ_M. The data in Figs. 1(a) and 1(b) are obtained for $P/\tau_M = 100$ and 8, respectively.

[18] S. W. Sides, P. A. Rikvold, and M. A. Novotny, Phys. Rev. Lett. **81**, 834 (1998).

[19] S. W. Sides, P. A. Rikvold, and M. A. Novotny, Phys. Rev. E **59**, 2710 (1999).

[20] D. T. Robb, P. A. Rikvold, A. Berger, and M. A. Novotny, Phys. Rev. E **76**, 021124 (2007).

[21] D. T. Robb, Y. H. Xu, O. Hellwig, J. McCord, A. Berger, M. A. Novotny, and P. A. Rikvold, Phys. Rev. B **78**, 134422 (2008).

[22] A. Berger, O. Idigoras, and P. Vavassori, Phys. Rev. Lett. **111**, 190602 (2013).

[23] D. T. Robb and A. Ostrander, Phys. Rev. E **89**, 022114 (2014).

[24] R. A. Gallardo, O. Idigoras, P. Landeros, and A. Berger, Phys. Rev. E **86**, 051101 (2012).

[25] M. Quintana and A. Berger, Phys. Rev. E **104**, 044125 (2021).

[26] N. D. Goldenfeld, *Lectures on Phase Transitions and the Renormalization Group* (Addison-Wesley, Reading, MA, 1992).

[27] P. Riego, P. Vavassori, and A. Berger, Phys. Rev. Lett. **118**, 117202 (2017).

[28] G. M. Buendía and P. A. Rikvold, Phys. Rev. B **96**, 134306 (2017).

[29] H. Park and M. Pleimling, Phys. Rev. E **87**, 032145 (2013).

[30] E. Vatansever and N. G. Fytas, Phys. Rev. E **97**, 012122 (2018).

[31] E. Vatansever and N. G. Fytas, Phys. Rev. E **97**, 062146 (2018).

[32] See Supplemental Material at http://link.aps.org/supplemental/10.1103/PhysRevLett.131.116701 for further details regarding experimental methods, data analysis, and data for thicker films that exhibit strong metamagnetic anomalies, which includes Refs. [33–39].

[33] O. Idigoras, U. Palomares, A. K. Suszka, L. Fallarino, and A. Berger, Appl. Phys. Lett. **103**, 102410 (2013).

[34] A. J. Bennett and B. R. Cooper, Phys. Rev. B **3**, 1642 (1971).

[35] H. J. G. Draaisma and W. J. M. de Jonge, J. Appl. Phys. **64**, 3610 (1988).

[36] Y. Millev and J. Kirschner, Phys. Rev. B **54**, 4137 (1996).

[37] I. A. Sergienko and E. Dagotto, Phys. Rev. B **73**, 094434 (2006).

[38] A. Hrabec, N. A. Porter, A. Wells, M. J. Benitez, G. Burnell, S. McVitie, D. McGrouther, T. A. Moore, and C. H. Marrows, Phys. Rev. B **90**, 020402(R) (2014).

[39] E. C. Stoner and E. P. Wohlfarth, Phil. Trans. R. Soc. A **240**, 599 (1948).

[40] O. Idigoras, A. K. Suska, P. Vavassori, B. Obry, B. Hillebrands, P. Landeros, and A. Berger, J. Appl. Phys. **115**, 083912 (2014).

[41] J. M. Marín Ramírez, E. Oblak, P. Riego, G. Campillo, J. Osorio, O. Arnache, and A. Berger, Phys. Rev. E **102**, 022804 (2020).

[42] M. Quintana, E. Oblak, J. M. Marín Ramirez, and A. Berger, Phys. Rev. B **102,** 094436 (2020).

[43] E. Oblak, P. Riego, L. Fallarino, A. Martínez-de-Guerenu, F. Arizti, and A. Berger, J. Phys. D **50,** 23LT01 (2017).

[44] E. Oblak, P. Riego, A. Garcia-Manso, A. Martínez-de-Guerenu, F. Arizti, I. Artetxe, and A. Berger, J. Phys. D **53,** 205001 (2020).

[45] C. Martin Valderrama, M. Quintana, A. Martínez-de-Guerenu, T. Yamauchi, Y. Hamada, Y. Kurokawa, H. Yuasa, and A. Berger, J. Phys. D **54,** 435002 (2021).

[46] C. Martin Valderrama, M. Quintana, A. Martínez-de-Guerenu, T. Yamauchi, Y. Hamada, Y. Kurokawa, H. Yuasa, and A. Berger, J. Phys. D **55,** 435007 (2022).

[47] A. Kimel *et al.*, J. Phys. D **55,** 463003 (2022).

[48] A. Arrott and J. E. Noakes, Phys. Rev. Lett. **19,** 786 (1967).

[49] P. Alvarez-Alonso, J. L. Sánchez Llamazares, C. F. Sánchez-Valdés, G. J. Cuello, V. Franco, P. Gorria, and J. A. Blanco, J. Appl. Phys. **115,** 17A929 (2014).

[50] J. Waters, A. Berger, D. Kramer, H. Fangohr, and O. Hovorka, J. Phys. D **50,** 35LT01 (2017).

[51] A. Aspelmeier, F. Gerhardter, and K. Baberschke, J. Magn. Magn. Mater. **132,** 22 (1994).

[52] Y. Li and K. Baberschke, Phys. Rev. Lett. **68,** 1208 (1992).

[53] F. Huang, M. T. Kief, G. J. Mankey, and R. F. Willis, Phys. Rev. B **49,** 3962 (1994).

[54] P. Cossio, J. Mazo-Zuluaga, and J. Restrepo, Physica (Amsterdam) **384B,** 227 (2006).

[55] L. Fallarino, E. López Rojo, M. Quintana, J. S. Salcedo Gallo, B. J. Kirby, and A. Berger, Phys. Rev. Lett. **127,** 147201 (2021).

[56] A. Hubert and R. Schäfer, *Magnetic Domains: The analysis of Magnetic Microstructures* (Springer-Verlag, Berlin, Heidelberg, New York, 1998), ISBN: 978-3540641087, 10.1007/978-3-540-85054-0.

[57] H. Park and M. Pleimling, Phys. Rev. Lett. **109,** 175703 (2012).